Materials Horizons

ROYAL SOCIETY OF CHEMISTRY

COMMUNICATION

View Article Online
View Journal | View Issue

Check for updates

Cite this: *Mater. Horiz.*, 2024, **11**, 2428

Received 24th November 2023,
Accepted 7th January 2024

DOI: 10.1039/d3mh01999c

rsc.li/materials-horizons

A flexible multimodal pulse sensor for wearable continuous blood pressure monitoring†

Shuo Tian, Liangqi Wang and Rong Zhu*

Monitoring of arterial blood pressure *via* cuffless pulse waveform measurement at the wrist has an important clinical value for the early diagnosis and prevention of cardiovascular disease. However, accurate measurement of the radial pulse waveform is challenging owing to its subtle, wideband, and preload-dependent variation characteristics. Evidence shows that uncertainties or variations of wearing pressure and skin temperature can cause artifact signals in wrist pulse measurements, thus degrading blood pressure estimate accuracy and hindering precise clinical diagnosis. Herein, we report a flexible multisensory pulse sensor utilizing natural piezo-thermic transduction of human skin in conjunction with thin-film thermistors for the accurately measuring radial artery pulse waves with high fidelity and good anti-artifact performance. The flexible pulse sensor achieved a wide pressure measuring range (228.2 kPa), low detection limit (4 Pa), good linearity (R^2 = 0.999), low hysteresis (2.45%), fast response (88 ms), and good durability and stability, thereby enabling accurate pulse measurement with high fidelity. The pulse sensor also monolithically integrated the simultaneous detections of skin temperature and wearing pressure for resisting artifact effects in pulse measurements. Through the fusion of multiple features extracted from the pulse waveform, wearing pressure, skin temperature and user's personal physical characteristics using an efficient multilayer perceptron, blood pressure is accurately estimated and good generalizability is achieved.

New concepts

Continuous blood pressure monitoring *via* the radial pulse has a high demand for personal healthcare. However, accurate measurement of the radial pulse waveform is challenging owing to its subtleness and susceptible to wearing pressure and skin temperature, which can bring about artifact signals aliasing in the pulse waveform. Herein, we propose a brand-new pressure sensing principle of human skin's piezo-thermic transduction, and develop a flexible multisensory pulse sensor to implement high-fidelity pulse waveform measurement. Leveraging natural piezo-thermic transduction of human-skin in conjunction with flexible thin-film thermoreceptors, our pulse sensor achieves superior performances with a wide pressure measuring range (228.2 kPa), low detection limit (4 Pa), high sensitivity, good linearity (R^2 = 0.999), low hysteresis (2.45%), fast response (88 ms), and good durability and stability, which enable accurate pulse measurement. In addition, the flexible pulse sensor monolithically integrates the perceptions of skin temperature and wearing pressure, enabling real-time compensation of artifact effects on pulse measurement. Blood pressure is accurately estimated and achieves good generalizability through the fusion of pulse features, wearing pressure, and skin temperature utilizing efficient multilayer perceptron. This study provides a new concept of human-skin transducer and, for the first time, implements integrated high-fidelity measurements of the pulse pressure wave, skin temperature, and wearing pressure to enable accurate wearable blood pressure monitoring with good generalizability.

1. Introduction

Abnormal blood pressure has become an acute health challenge globally. In recent years, the number of individuals with hypertension has increased rapidly, leading to a significant surge in the risk of cardiovascular disease.[1] Concurrently, systemic and orthostatic hypotension have emerged as significant risk factors with adverse outcomes.[2] Hence, it is crucial for individuals to undergo regular blood pressure checkups to prevent various complications associated with abnormal blood pressure. Personal blood pressure monitoring can enable the early diagnosis and daily monitoring of cardiovascular disease.

A range of blood pressure monitoring techniques have been developed. Traditional blood pressure monitoring primarily relies on manual cuff-based auscultation or oscillometry techniques, which are arduous to continuously monitor and not portable. In response to the limitations of cuff-based measurement methods, researchers have proposed an assortment of non-intrusive measurement approaches for continuous blood pressure monitoring that can be applied with wearable devices,

---

State Key Laboratory of Precision Measurement Technology and Instrument, Department of Precision Instrument, Tsinghua University, Beijing, 100084, China. E-mail: zr_gloria@mail.tsinghua.edu.cn

† Electronic supplementary information (ESI) available. See DOI: **https://doi.org/10.1039/d3mh01999c**

including pulse transit time (PTT), pulse wave velocity (PWV), pulse wave analysis (PWA), and ultrasound methods.[3]

The PTT, PAT, and PWV methods are fundamentally similar in principle. Blood pressure impacts vascular tone and arterial wall rigidity, which subsequently influences the PTT, while the PTT can be regressed to blood pressure with suitable models. However, PTT-like methods are data-driven modeling methods, and have poor generalizability. The ultrasound method records the diameter of pulsating vessels, but it requires calibration with a cuffed sphygmomanometer.[4] The PWA method extracts features from the pulse waveform and maps them to the blood pressure through a regression model. Recently, PWA methods have gained increasing interest in combination with machine learning.[5–8]

Devices that record pulse waveforms include photoplethysmography (PPG),[9–11] pressure sensors,[12–15] impedance cardiography (ICG),[16] strain sensors,[17,18] and others. PPG sensors are the most commonly-used wearable pulse sensors, but are vulnerable to several factors, such as light interference and skin color.[19,20] Conversely, pressure sensors are immune from light and color factors. However, the wrist pulse pressure waveform is influenced by body temperature[21,22] and the wearing preload pressure, which can cause artifact signals aliasing in the pulse waveform.[23] Conventional pulse pressure sensors have certain limitations in their quest for precise pulse measurements. Piezoresistive sensors are prone to temperature-induced interference in their measurement outcomes.[24] Pressure capacitive sensors are heavily influenced by parasitic capacitance and environmental interference.[25] Piezoelectric sensors and frictional electrical sensors have difficulty in accurately measuring the pulse waveform with high fidelity due to their band-limited problem,[26] particularly hardly detect static and low-frequency pressure signals. These technique issues significantly impact the estimate accuracy of blood pressure from their pulse measurements.

Here, we report a novel flexible multisensory pulse sensor utilizing thin-film thermoreceptors to implement the multimodal detection of the pulse pressure waveform, skin temperature, and wearing pressure simultaneously. In virtue of the natural piezo-thermic transduction of human skin in conjunction with highly-sensitive thin-film thermometry, the sensor could achieve accurate measurement based on the radial pulse waveform with high fidelity. We further developed a wearable wristwatch for use with the pulse sensor, by which tens of pulse waveform features are extracted and combined with the parameters of the wearing pressure and skin temperature as well as the user's physical characteristics (height, weight, age, body mass index, *etc.*) to estimate blood pressure in real time using a machine-learning algorithm. The proposed multimodal pulse sensor enabled continuous blood pressure monitoring with high accuracy and good generalizability.

2. Results and discussion

2.1. Working principle of the pulse sensor and wearable device

Through the periodic contraction and diastole of a heart, blood flow causes alterations in blood vessel diameter and intravascular pressure, resulting in arterial pulsations perceptible at the body surface known as pulse waves. The pulse wave signal from the radial artery can be regressed to brachial blood pressure, thereby serving as an additional indicator for health monitoring and medical advice. High fidelity and high sensitivity in pulse wave measurements are of great significance in blood pressure estimation. In this regard, we propose a flexible multimodal pulse sensor utilizing thin-film thermoreceptors to accurately detect the wrist pulse wave, skin temperature, and wearing pressure simultaneously (Fig. 1a). The proposed pulse sensor, inspired by traditional Chinese medicine (TCM), emulates the preload pressure applied by the fingertips during pulse diagnosis. Studies have indicated that, aside from blood flow, changes in the diameter of terminal arterial vessels due to the body temperature and preload pressure during monitoring can affect the pulse signal. Therefore, skin temperature and pre-pressure effects should be considered when conducting pulse wave analysis (Fig. 1a). Our sensor combined the multimodal detections of the pulse pressure wave, skin temperature, and preload pressure (*i.e.*, wearing pressure) to ultimately enable the high accuracy of blood pressure estimates. The pulse sensor was further made into a wristwatch device to be worn on a human wrist (Fig. 1b), enabling concurrent measurements of the blood pressure, pulse wave, skin temperature, and heart rate. In order to ensure the pulse sensor is best placed on the radial artery, the wearer can adjust the location of the pulse sensor on the wrist to maximize the detected pulse signal.

The flexible pulse sensor detects the pulse pressure wave, skin temperature, and wearing pressure by using a flexible thin-film thermal sensing layer appressed with piezo-thermic materials (Fig. 1c and 2a). Piezo-thermic transduction refers to the conversion of a pressure stimulus to the heat conductance change of a material. When a pressure impresses on a piezo-thermic material, its thermal conductivity will be changed and can be detected by a heated thermosensitive film on the sensing layer. Human skin is a natural piezo-thermic material. When a pressure is applied onto human skin, the effective thermal conductivity of human skin changes due to the changes in the relative distribution and volume fraction of components such as the epidermis and dermis in the human skin, as well as the subcutaneous tissue beneath the dermis.[27] Hence, the intricate composition of the skin material/structure renders it a discerning piezo-thermic substance, converting contact pressure into a change in its effective thermal conductivity. Specifically, in the case of superficial arteries in the human body, the arterial vasculature undergoes significant periodic contraction and diastole due to the pulsation of the heart and the circulation of the blood flow. When the blood vessels dilate, they compress the superficial skin tissue above them, thereby enhancing their thermal conductivity and resulting in a greater heat loss of the heated thermosensitive film (Fig. 1c); while the relaxation of the superficial skin tissue corresponding to vasoconstriction causes a decrease in the skin thermal conductivity and thus a decrease in the heat loss of the heated thermosensitive film. Thanks to the inherent piezo-thermic transduction of human skin and the flexible thin-film sensing layer being well appressed with human skin, and the additional porous silver-particle reinforced PDMS

(PDMS/Ag) on the back, which serves as not only another artificial piezo-thermic material but also a hold-down element (Fig. 2a), the pressure/temperature sensitivity and measuring stability are greatly enhanced. The porous PDMS/Ag is an excellent piezo-thermic material, because the thermal conductivity of air is much lower than that of PDMS/Ag,[28] and external pressure can compress the porous PDMS/Ag and decrease the internal air, thus altering its thermal conductivity.

As mentioned above, the pulse sensor consisted of a flexible sensing layer sandwiched between two piezo-thermic materials of human skin and porous PDMS/Ag (Fig. 2a). The flexible sensing layer contained two concentric annular Cr/Pt thin films (~100 nm thick) as thermosensitive elements deposited on a polyimide substrate (50 μm). The inner thermosensitive film (thermistor, 40 Ω) was electrically heated to a higher temperature (~5 K) than its surroundings, generating a spherical thermal field interacting with the surroundings. The outer thermosensitive film (450 Ω) functioned as a temperature sensor to detect skin temperature. The detailed fabrication processes of the flexible sensing layer and the porous silver-particle reinforced PDMS are described in ESI† Note S1 and Note S2. The inner and outer thermistors R_h and R_c on the flexible sensing layer were connected to a custom-designed constant temperature difference (CTD) circuit to implement the pressure and temperature detections as well as the temperature and strain compensations for the pressure measurement[29] (Fig. 2a and b, details in ESI† Note S3). In other words, the pulse sensor was capable of independent and simultaneous measurements of the pressure and temperature. Specifically, the thermal field generated by the inner thermistor R_h transfers heat toward the surrounding piezo-thermic materials. As the pressure increases, the thermal conductivity of the piezo-thermic materials rises, thereby augmenting the power of the circuit to uphold a constant temperature difference between R_h and R_c. This results in an increase in the voltage (Output_P) at the top of the Wheatstone bridge. Therefore, the pressure output refers to the top voltage (Output_P) of the bridge. At the same time, the outer thermistor R_c with less Joule heat works as a temperature sensor. The

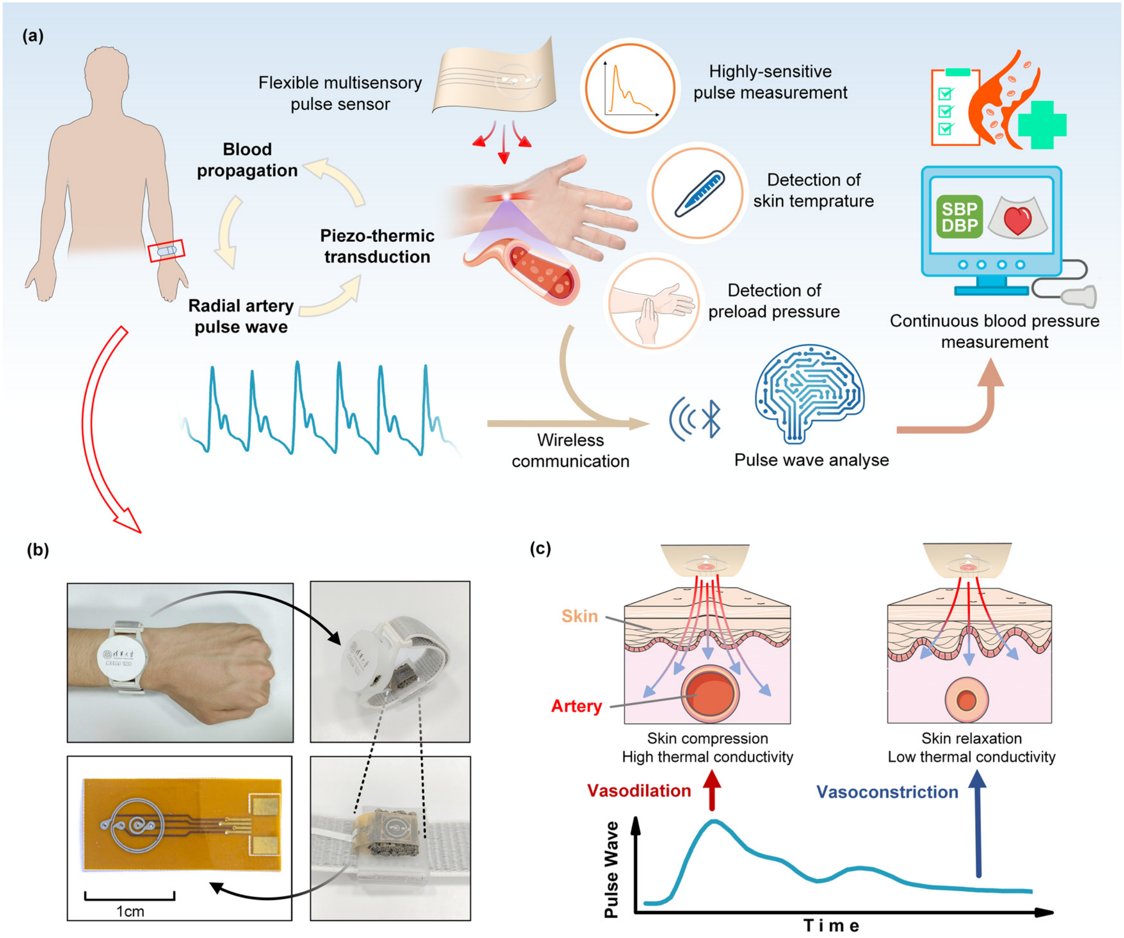

Fig. 1 Working principles of the pulse sensor and blood pressure measurement. (a) Schematic diagrams of the sensor principle and blood pressure measurement. The pulse sensor detects the pulse pressure waveform using natural piezo-thermic transduction of human skin in conjunction with a thin-film thermoreceptor. Multimodal detections of the pulse wave, skin temperature, and preload pressure are monolithically integrated in the pulse sensor. Multimodal sensing information is utilized to estimate blood pressure by a machine-learning approach. (b) Prototypes of the pulse sensor and wearable wristwatch. (c) Schematic diagram of a human skin piezo-thermic transduction incorporated with a heated thermosensitive film for pulse pressure measurement.

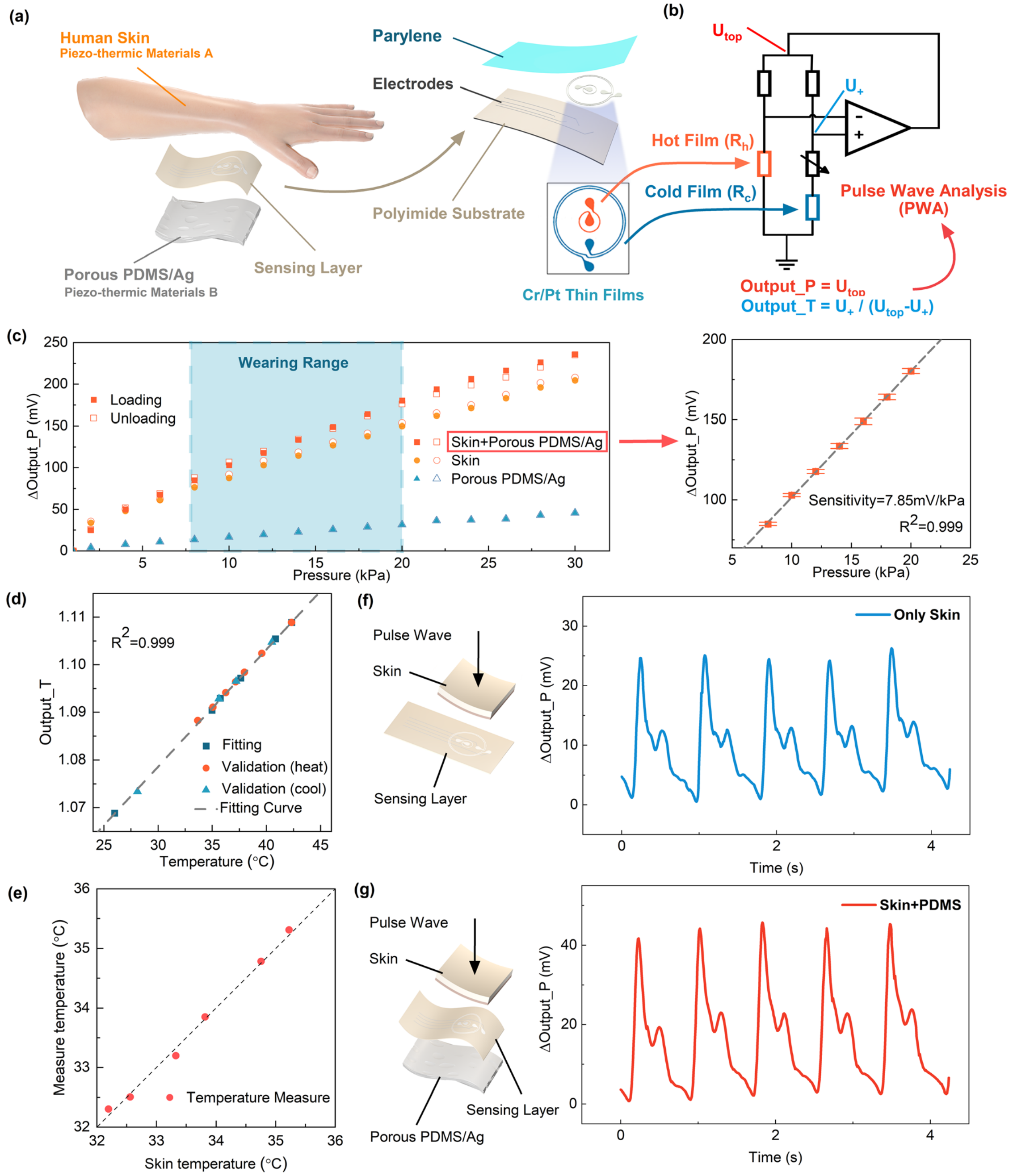

Fig. 2 Structure configuration and characteristics of the pulse sensor. (a) Structure configuration of the pulse sensor. (b) Schematic diagram of the constant temperature differential (CTD) circuit. The pressure and temperature signals are utilized for subsequent pulse wave analysis to estimate blood pressure. (c) Pressure responses of the pulse sensor with different piezo-thermic configurations, including human skin, porous PDMS/Ag, and a combination of human skin and porous PDMS/Ag. The pressure ranging 8–20 kPa is the daily wearing pressure range. (d) Temperature response of the pulse sensor. (e) Temperature measurement of the pulse sensor. (f) Detected pulse waves using the pulse sensor with only human skin. (g) Detected pulse waves using the pulse sensor with a combination of human skin and porous PDMS/Ag.

temperature output refers to the ratio (Output_T), as shown in Fig. 2b. Therefore, the pulse sensor was endowed with the capability for pressure and temperature sensing.

Fig. 2c depicts the pressure responses of the pulse sensor under external pressure stimuli in the range covering the daily wearing pressure. We compared the pressure sensing characteristics of the pulse sensor with three piezo-thermic configurations, *i.e.*, with only porous PDMS/Ag, with only human skin, and with human skin and porous PDMS/Ag on two sides of the flexible sensing layer, respectively. The comparison results shown in Fig. 2c indicate that the piezo-thermic configuration with a combination of human skin and porous PDMS/Ag achieved the highest sensitivity of 7.85 mV kPa^{-1}, the best linearity (R^2 = 0.999), and the lowest hysteresis error of 2.45%, which could ensure high-fidelity pulse measurements. The pulse sensor also exhibited a wide pressure measurement range of 0–228.2 kPa, a lower detection limit of 4 Pa, a fast response time of 88 ms, and good durability and stability, as shown in ESI† Note S4. The temperature sensing response (Output_T), shown in Fig. 2d and e, indicated the temperature measurement errors were less than 0.2 °C. Details of the temperature measurement are described in ESI† Note S5.

Furthermore, we measured the pulse waves at the radial artery using the pulse sensors with different piezo-thermic configurations. Fig. 2f shows the pulse waves measured by using only human skin as a single piezo-thermic material, while Fig. 2g shows the pulse waves measured by using a combination of human skin and porous PDMS/Ag as dual piezo-thermic layers. The comparison result again indicated the dual piezo-thermic layers could effectively enhance the pulse pressure sensitivity.

2.2. Concurrent measurements of the pulse wave, wearing pressure, and skin temperature

As blood courses through the vasculature, it imposes a force on the vessel walls, known as blood pressure. The blood pressure during cardiac contraction is designated as the systolic blood pressure (SBP), whereas the blood pressure during heart resting is called the diastolic blood pressure (DBP). The medically referenced concept of blood pressure refers mainly to the aortic blood pressure, and it is arduous to gauge this value directly and non-invasively. Therefore, peripheral arteries, such as the brachial and carotid arteries, are usually measured as substitutes.[30] Within the arterial network, the diastolic and mean arterial pressures persist as stable, while the systolic pressure is augmented as the artery narrows, thus demonstrating a variable pressure waveform as it travels to the end of the artery.[31] Furthermore, variations in the terminal arterial diameter resulting from body temperature, as well as the pre-pressure applied to the artery during monitoring, can affect the pulse signals. Leveraging the relationship between the radial blood pressure and brachial blood pressure, we measured the radial artery's pulse waveform, accounting for the associated influences of skin temperature and preload pressure, to retroactively estimate the brachial blood pressure.

Although numerous wearable sensors can enable detection of pressure waves, continuous pulse recording in dynamic, realistic environments remains impractical due to the need for manual pressure to be applied to obtain high-quality pulse waveform signals during daily activities.[12] In our work, a flexible sensing layer sandwiched between natural human skin and porous PDMS/Ag allowed detection directly on human skin, providing the sensor with good pressure and temperature sensitivity. In addition, the porous PDMS on the back of the sensing layer played a role not only in piezo-thermic transduction, but also a pressing role on the wristwatch device, akin to the fingertip pressure applied during pulse diagnosis in traditional Chinese medicine. Details of the device design are provided in ESI† Note S6.

Considering the influence of the wearing pressure on the pulse measurement, the pressure exerted on the radial artery can be classified as superficial (Fu), medium (Zhong), and deep (Chen) in order of the increasing contact pressure for traditional Chinese pulse diagnosis. We detected the pulse signals under increasing contact pressures from Fu to Zhong and then to Chen, as depicted in Fig. 3a. The pulse signal evolved from weak to strong as the wearing pressure increased from

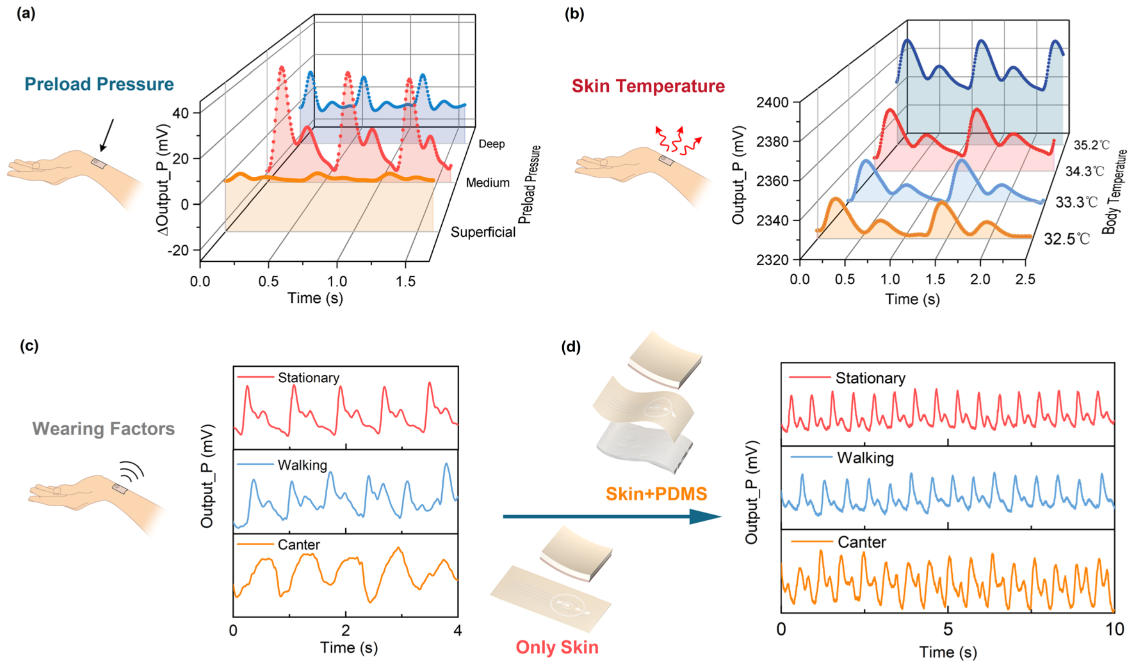

Fig. 3 Factors influencing the pulse wave measurement. (a) Effects of preload pressures on the pulse wave measurement. (b) Effects of skin temperatures on the pulse wave measurement. (c) Effects of body movements on the pulse wave measurement using the pulse sensor with only human skin. (d) Effects of body movements on the pulse wave measurement using the pulse sensor with a combination of human skin and porous PDMS/Ag.

superficial to medium, along with discernible peaks becoming apparent. When the wearing pressure exceeded the medium range, the pulse signal was suppressed, and waveform distortion occurred. Our pulse sensor was designed to gauge the wearing pressure at this juncture based on the DC component (*i.e.*, baseline) of the pulse pressure signal. The pulse sensor extracts the pulse wave by the AC component at a wearing pressure of 8–20 kPa.

Although there is no direct link between body temperature and aortic blood pressure, the temperature of the extremities impacts the vasoconstriction of the peripheral arteries and consequently influences the measurement of the pulse. To investigate the impact of skin temperature, we monitored the corresponding changes of the pulse signals while gradually altering the skin temperature through local environmental exposure, as shown in Fig. 3b. As the skin temperature increased, the vasoconstriction in the radial artery decreased, and the pulse signal became more pronounced and less distorted. Therefore, it is critical to factor in the skin temperature to the pulse wave analysis for the blood pressure regression.

Wearing factors also affect the pulse measurements. For instance, pulse wave signals are usually distorted during exercise. Fig. 3c shows the pulse wave measurements under different exercises using the pulse sensor with only human skin as the piezo-thermic layer. The pulse wave measurement was good at the quiescent state, but severely distorted during walking and completely lost its characters during cantering. Fig. 3d shows the pulse sensor using a combination of human skin and porous PDMS membrane as dual piezo-thermic layers was capable of detecting the pulse wave very well, even under walking and cantering. The porous PDMS on the back helped to amplify the pulse signals, and could effectively restrain motion artifacts as well.

We compare different types of pressure sensors in Table S1 (ESI†). Our pulse sensor utilizes natural piezo-thermic transduction of the human skin in conjunction with thin-film thermistors to implement the simultaneous detections of the pulse pressure waveform, skin temperature, and wearing pressure with a broad measurement range, high sensitivity, and good linearity.

2.3. Feature extraction and data fusion for blood pressure estimation

Fig. 4a and b illustrate schematics of the proposed blood pressure (BP) estimation method, employing a data fusion algorithm, which encompasses the following sequential steps: 1. collection of dual-channel signals from the pulse sensor, comprising the pressure signal (Output_P) and the temperature signal (Output_T); 2. extraction of the pulse waveform features and wearing pressure from the signal Output_P and estimation

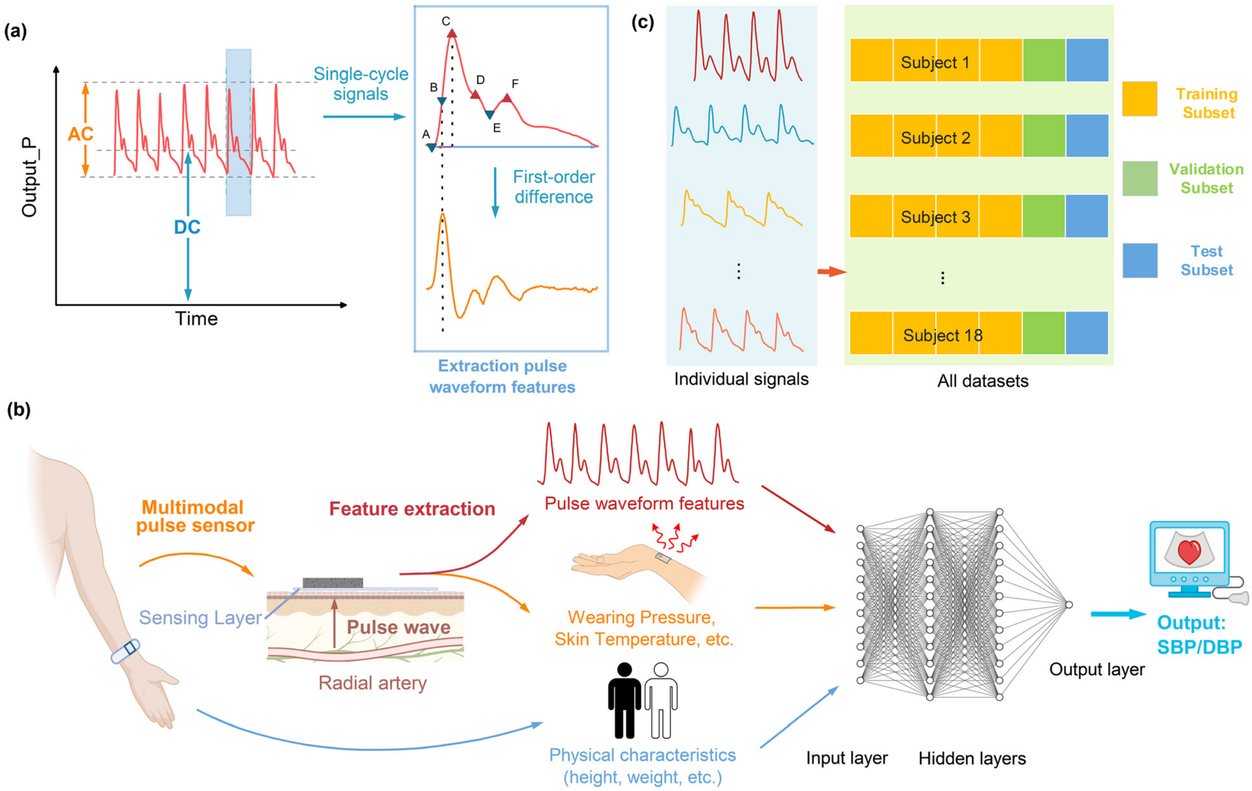

Fig. 4 Feature extraction and fusion for blood pressure estimation. (a) Extraction of the pulse wave features from the detected pulse pressure wave. Point A corresponds to the pulse wave trough, B refers to the point of the maximum slope during the ascending period, C refers to the percussion wave, D refers to the tidal wave, E refers to the dicrotic notch, and F refers to the dicrotic wave. (b) Blood pressure estimation using an MLP network input with the pulse waveform features, skin temperature, wearing pressure, and personal physical characteristics. (c) Six-fold cross-validation to evaluate the blood pressure estimation.

of the skin temperature from the signal Output_T, which are subsequently combined with individual physical characteristics (weight, height, age, gender, and body mass index BMI); 3. estimation of the systolic blood pressure (SBP) and diastolic blood pressure (DBP) utilizing a multilayer perceptron (MLP) model.

Continuous blood pressure measurement was conducted by wearing our wristwatch device on the wrist of a subject, while the ground truth blood pressure was measured synchronously using a commercial cuff-based blood pressure monitor, as depicted in Fig. 1b. The pressure signal (Output_P) and the temperature signal (Output_T) of the pulse sensor were collected at a sampling frequency of 125 Hz. The detected pulse waveform signal is shown in Fig. 2g. At the same time, a PPG signal was collected at a sampling frequency of 1000 Hz by the test subject wearing a PPG sensor at their fingertip for subsequent comparison analyses. In the data processing, a 30-s window with a 5-s shift (25-s overlap) was applied to estimate the SBP and DBP every 5 s using the MLP model. The waveform characteristics of each pulse cycle within 30 s were extracted from the sensor signal by filtering and then averaged to estimate the SBP and DBP (details in ESI† Note S7).

We extracted 28 blood pressure-related features from the pressure and temperature signals referring to the literature.[5–7,31,32] The features were extracted from every cardiac period in each 30-s window, and the mean value was calculated as well. The extracted features contained both time-domain and frequency-domain features with theoretical bases, and their detailed definitions and calculations are described in ESI† Note S8. The pulse waveform features involved amplitude-related and time-related features. For amplitude-related pulse waveform features, we incorporated the percussion wave and minimum pressure corresponding to the systolic and diastolic blood pressure, as well as the dicrotic wave and dicrotic notch corresponding to the resistance of the posterior vascular network. Tidal wave was not included in the feature extraction due to individual differences in its observation. For the time-related pulse waveform features, there is not yet a well-established theory for correlating blood pressure with pulse time-domain characteristics. Therefore, we selected the time-domain features that have been reported to be well correlated with blood pressure referring to the literature. The weights of the features were optimized through machine learning for blood pressure estimation. We further combined 28 features of the pulse sensor signals with the subject's physical characteristics (heart rate, age, height, weight, BMI index, gender), for a total of 33 features, to enable data fusion for using the MLP model for estimating continuous blood pressure.

Owing to the intricate interrelations among diverse signal features and blood pressure, a machine-learning methodology is commonly employed to establish a correlation model interfacing multi-features and blood pressure. In this work, a neural network of MLP was embraced to construct the data fusion paradigm due to the model's simple structure and regression accuracy. The utilization of the MLP was directed toward the estimation of blood pressure, as shown in Fig. 4b. The multi-features extracted from the pulse signals and the personal physical characteristics were the inputs for the MLP, and the output was the SBP or DBP. The hidden layer was set as 2 layers, and the numbers of neurons were optimized to be 80 and 20. Behind each hidden layer, there was a dropout layer (dropout layer 10%) to reduce overfitting and increase generalization ability. (The optimization process for the MLP is described in ESI† Note S9). Rectified linear units (ReLUs) were set as the activation function of the hidden layer, while the loss function was ascribed to the mean squared error (MSE). The optimization mechanism adopted was the Adam algorithm, with a learning rate specified at 0.001. As a safeguard against overfitting, an appended punitive term in the form of L2 regularization was incorporated into the loss function, thereby orchestrating weight attenuation, and circumscribing the summation of neuron weight squares.

2.4. Experiment of blood pressure measurement

To verify the effectiveness of the blood pressure measurement using our wristwatch with the pulse sensor, a total of N = 18 healthy subjects (age: 24.8 ± 3.1 years old, BMI: 21.1 ± 2.6 kg m^{-2}, N = 13 male and N = 5 female) participated in the experiment. In total, 260 datasets of blood pressure measurements from the 18 subjects were collected in the morning and afternoon. To validate the generalization of the method, the subjects removed and put the wristwatch device back on between different measurements. Details of the blood pressure measurements are provided in ESI† Note S10.

The MLP model was trained using 6-fold cross-validation to evaluate the blood pressure estimation, as illustrated in Fig. 4c. Also, 66% of the total datasets of the blood pressure measurements were used in turn as the training set to build the model, while another 17% of the datasets were used as the validation set, and the other remaining 17% were taken as the validation set. The estimated blood pressure values are summarized for the statistical assessments (ME and SD, defined in ESI† Note S11).

We compared two sets of input parameter configurations, *i.e.*, with and without the parameters of the wearing pressure and skin temperature, in the blood pressure estimations. The comparison results are shown in Fig. 5.

2.5. Results of blood pressure estimation

The experimental results shown in Fig. 5a and b (marked in blue) indicate that the estimation errors were −0.03 ± 5.56 mmHg (ME ± SD) for the SBP and 0.12 ± 3.91 mmHg (ME ± SD) for the DBP using the multimodal parameters of the pulse wave features, wearing pressure, and skin temperature as the inputs of the MLP model. A Bland–Altman plot was used to evaluate the agreement between the estimated blood pressure and the true blood pressure, as depicted in Fig. 5c and d (marked in blue). The limit of agreement (LOA) is represented as $[\mu - 1.96\sigma, \mu + 1.96\sigma]$, where μ and σ denote the mean and standard deviation of the difference between the estimated blood pressure and the true blood pressure, respectively. The LOA was [−10.92, 10.87] mmHg for the SBP, and [−7.61, 7.71] mmHg for the DBP. There were a few outliers for both estimates of the SBP and DBP. For comparison, the estimate results

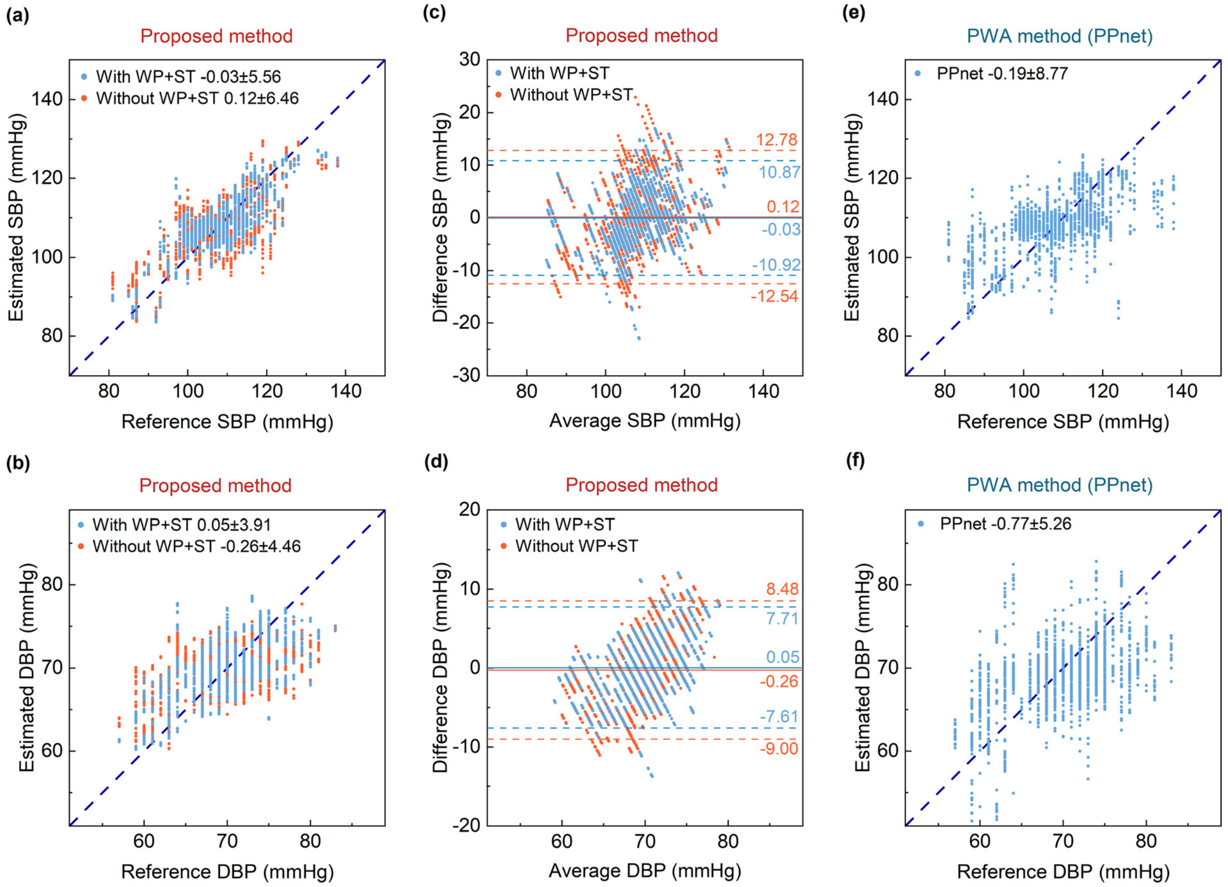

Fig. 5 Scatter plots and Bland–Altman plots of SBP and DBP estimates for 18 subjects. (a) Scatter plot between the reference SBP and estimated SBP using the proposed method with the multimodal pulse sensor. Blue points are the blood pressure estimation results using the multimodal features of the pulse wave features, wearing pressure, and skin temperature features and physical characteristics as the inputs of the MLP mode. Orange points are the blood pressure estimation results without inputting the wearing pressure and skin temperature features into the MLP model. WP refers to the wearing pressure and ST refers to the skin temperature. (b) Scatter plot between the reference DBP and the estimated DBP using the proposed method with the multimodal pulse sensor. (c) Bland–Altman plot of the estimated SBP using the proposed method with the multimodal sensor. (d) Bland–Altman plot of the estimated DBP using the proposed method with the multimodal pulse sensor. (e) Scatter plot between the reference SBP and the estimated SBP using the PPG-based PWA method (PPnet). (f) Scatter plot between the reference DBP and the estimated DBP using the PPG-based PWA method (PPnet).

without inputting the wearing pressure and skin temperature into the MLP model are also shown in Fig. 5a and b (marked in orange). The estimation errors were 0.12 ± 6.46 mmHg for the SBP and -0.26 ± 4.46 mmHg for the DBP. Additionally, the Bland–Altman plots are shown in Fig. 5c and d (marked in orange), for which the LOA was [−12.54,12.78] mmHg for the SBP and [−9.00, 8.48] mmHg for the DBP. A comparison of the results indicated that taking the wearing pressure and skin temperature into account effectively improved the accuracy of the blood pressure estimation. The estimation errors of the SBP and DBP achieved the standard of AAMI ($\text{ME} < \pm 5$ mmHg and $\text{SD} < 8$ mmHg).

As mentioned above, pulse waveform analysis (PWA) using a PPG sensor is a commonly-used method in current wearable blood pressure monitoring. To showcase the superiority of our pulse sensor and proposed blood pressure estimate method, we compared the results of our blood pressure estimates with those using the PPG-based PWA method. Consequently, a PPG sensor worn at the fingertip was employed synchronously to detect the volume pulse waves of the subjects. Utilizing the PPG data, a PPnet network[8] combining a convolutional neural network (CNN), long short-term memory (LSTM), and a dense layer (see details in ESI† Note S12) was trained to estimate the blood pressure. The PWA network takes the detected PPG waveform as the inputs and takes either the systolic blood pressure (SBP) or diastolic blood pressure (DBP) as the outputs. Fig. 5e and f show the results of the PPG-based PWA method in terms of 6-fold cross-validation. The PWA method provided an estimation error of -0.19 ± 8.77 mmHg for the SBP and -0.77 ± 5.26 mmHg for the DBP. It was noted that the blood pressure estimates from the PPG-based PWA method displayed greater dispersion compared to the results using our multimodal pulse sensor. Additionally, our proposed data fusion method using the MLP network inputted with the extracted pulse wave features significantly lowers the fusion model complexity, and reduces the computation load and enhances the estimate efficiency. Besides the blood pressure estimate, the wristwatch device also provides for real-time monitoring of the pulse wave, skin temperature, and heart rate for comprehensive health monitoring and assessment, as shown in Fig. S2 (ESI†).

To comprehensively compare our device with other competing approaches for wearable continuous blood pressure measurements,[8,12,15,33–45] we summarize the state-of-the-art methods in Table S2 (ESI†). Most methods evaluate the blood pressure measurement accuracy through subject-specific calibration without considering the generalizability of the models. The comparison shows that our proposed device achieved a high accuracy of continuous blood pressure measurement and good generalizability. The improvement of the BP estimation mainly stems from two aspects. First, the real-time monitoring of the wearing pressure and skin temperature provide multimodal sensing information for accurate blood pressure estimation. Second, feature extraction attenuates the effect of individual variability on blood pressure estimation, which arises from the variation in peripheral resistance among individuals, leading to distinct pulse waveforms in different subjects. Even for the same individual, factors like exercise and temperature fluctuations would induce changes in peripheral resistance, causing the pulse waveform to fluctuate over time. Waveform-based blood pressure estimation is also more susceptible to environmental disturbances. In comparison, our estimate approach based on feature extraction was proven to be more robust in blood pressure estimation.

3. Conclusion

In this paper, we report a flexible multimodal pulse sensor for cuffless continuous blood pressure measurements. Pulse pressure waveforms could be accurately measured with high fidelity using the natural piezo-thermic transduction of human skin in conjunction with flexible thin-film thermoreceptors. The skin temperature and wearing pressure were concurrently detected by the pulse sensor during pulse wave monitoring, thus enabling anti-interference pulse measurements. The pulse pressure waveform was utilized to extract multiple key features fused with the skin temperature and wearing pressure to achieve accurate blood pressure estimation. We further developed a wristwatch utilizing the pulse sensor, which can be worn on the wrist to implement the real-time monitoring of the blood pressure, pulse wave, skin temperature, and heart rate for comprehensive health monitoring and assessment. Multi-subject experiments validated the effectiveness and showcase the promising potential of the proposed pulse sensor and wearable device in personal healthcare applications.

Experiments performed in this study involving human participants were approved by the Institution Review Board of Tsinghua University (No. 20180009). Informed consent was obtained from human subjects to use their images and conduct the experiments described in this paper.

Data availability

The data that support the findings of this study are available from the corresponding author upon reasonable request.

Author contributions

Rong Zhu: conceptualization, methodology, writing – reviewing and editing, supervision, funding acquisition. Shuo Tian: methodology, software, validation, investigation, writing – original draft preparation. Liangqi Wang: software, validation, investigation.

Conflicts of interest

The authors declare no competing interests.

Acknowledgements

This work was supported by the National Natural Science Foundation of China (Grant No. 51735007) and the Beijing Natural Science Foundation (3191001).

References

1 S. Krokstad, *Lancet*, 2022, **399**, 520.

2 G. Rivasi and A. Fedorowski, *Minerva Med.*, 2022, **113**, 251–262.

3 J. Solà and R. Delgado-Gonzalo, Cham: Springer, 2019.

4 C. Wang, X. Li, H. Hu, L. Zhang, Z. Huang, M. Lin, Z. Zhang, Z. Yin, B. Huang and H. Gong, *Nat. Biomed. Eng.*, 2018, **2**, 687–695.

5 K. H. Huang, F. Tan, T. D. Wang and Y. J. Yang, *Sensors*, 2019, **19**(4), 484.

6 F. Miao, N. Fu, Y. T. Zhang, X. R. Ding, X. Hong, Q. He and Y. Li, *IEEE J. Biomed. Health Inf.*, 2017, **21**, 1730–1740.

7 F. Miao, Z. D. Liu, J. K. Liu, B. Wen, Q. Y. He and Y. Li, *IEEE J. Biomed. Health Inf.*, 2020, **24**, 79–91.

8 M. Panwar, A. Gautam, D. Biswas and A. Acharyya, *IEEE Sens. J.*, 2020, **20**, 10000–10011.

9 Z. R. Yi, W. M. Zhang and B. Yang, *J. Micromech. Microeng.*, 2022, **32**(10), 103003.

10 M. Elgendi, R. Fletcher, Y. B. Liang, N. Howard, N. H. Lovell, D. Abbott, K. Lim and R. Ward, *NPJ Digital Med.*, 2019, **2**(1), 60.

11 X.-R. Ding, Y.-T. Zhang, J. Liu, W.-X. Dai and H. K. Tsang, *IEEE Trans. Biomed. Eng.*, 2016, **63**, 964–972.

12 S. Gong, L. W. Yap, Y. Zhang, J. He, J. Yin, F. Marzbanrad, D. M. Kaye and W. Cheng, *Biosens. Bioelectron.*, 2022, **205**, 114072.

13 K. Y. Meng, J. Chen, X. S. Li, Y. F. Wu, W. J. Fan, Z. H. Zhou, Q. He, X. Wang, X. Fan, Y. X. Zhang, J. Yang and Z. L. Wang, *Adv. Funct. Mater.*, 2019, **29**(5), 1806388.

14 Y. S. Oh, J.-H. Kim, Z. Xie, S. Cho, H. Han, S. W. Jeon, M. Park, M. Namkoong, R. Avila, Z. Song, S.-U. Lee, K. Ko, J. Lee, J.-S. Lee, W. G. Min, B.-J. Lee, M. Choi, H. U. Chung, J. Kim, M. Han, J. Koo, Y. S. Choi, S. S. Kwak, S. B. Kim, J. Kim, J. Choi, C.-M. Kang, J. U. Kim, K. Kwon, S. M. Won, J. M. Baek, Y. Lee, S. Y. Kim, W. Lu, A. Vazquez-Guardado, H. Jeong, H. Ryu, G. Lee, K. Kim, S. Kim, M. S. Kim, J. Choi, D. Y. Choi, Q. Yang, H. Zhao, W. Bai, H. Jang, Y. Yu, J. Lim, X. Guo, B. H. Kim, S. Jeon, C. Davies, A. Banks, H. J. Sung,

Y. Huang, I. Park and J. A. Rogers, *Nat. Commun.*, 2021, **12**, 5008.

15 J. Kim, E.-F. Chou, J. Le, S. Wong, M. Chu and M. Khine, *Adv. Healthcare Mater.*, 2019, **8**, e1900109.

16 Y. Zheng, C. C. Y. Poon, B. P. Yan and J. Y. W. Lau, *J. Med. Syst.*, 2016, **40**, 1–11.

17 S. Zhang, Y. Zhou, A. Libanori, Y. Deng, M. Liu, M. Zhou, H. Qu, X. Zhao, P. Zheng, Y.-L. Zhu, J. Chen and S. C. Tan, *Nat. Electron.*, 2023, **6**, 338–348.

18 S. Li, H. Wang, W. Ma, L. Qiu, K. Xia, Y. Zhang, H. Lu, M. Zhu, X. Liang, X.-E. Wu, H. Liang and Y. Zhang, *Sci. Adv.*, 2023, **9**, eadh0615.

19 K. Y. Meng, X. Xiao, W. X. Wei, G. R. Chen, A. Nashalian, S. Shen and J. Chen, *Adv. Mater.*, 2022, **34**(21), 2109357.

20 H.-J. Yeom, *The Journal of the Institute of Internet, Broadcasting and Communication*, 2011, **11**, 319–324.

21 M. H. Alali, L. C. Vianna, R. A. I. Lucas, R. T. Junejo and J. P. Fisher, *J. Appl. Physiol.*, 2020, **129**, 1373–1382.

22 T. Yan, S. Zhang, L. Yang, Y. Yang and X. Li, *Int. J. Bioautom.*, 2013, **17**, 91–96.

23 Y. Fu, S. Zhao, L. Q. Wang and R. Zhu, *Adv. Healthcare Mater.*, 2019, **8**(17), 1900633.

24 C. Liu, L. Xu, L. Y. Kong, Y. Q. Xu, W. Zhou, Q. P. Qiang, L. L. Tian, W. B. Chen, M. S. Cai, T. C. Lang, T. Han and B. T. Liu, *J. Mater. Chem. C*, 2022, **10**, 13064–13073.

25 K. H. Ha, W. Y. Zhang, H. Jang, S. M. Kang, L. Wang, P. Tan, H. Hwang and N. S. Lu, *Adv. Mater.*, 2021, **33**, 12.

26 S. D. Ma, J. Tang, T. Yan and Z. J. Pan, *IEEE Sens. J.*, 2022, **22**, 7475–7498.

27 L. Q. Wang, S. Q. Liu, G. Z. Li and R. Zhu, *Biosens. Bioelectron.*, 2021, **188**, 8.

28 S. Zhao and R. Zhu, *Adv. Mater. Technol.*, 2017, **2**, 9.

29 L. Q. Wang, R. Zhu and G. Z. Li, *ACS Appl. Mater. Interfaces*, 2020, **12**, 1953–1961.

30 C. M. McEniery, J. R. Cockcroft, M. J. Roman, S. S. Franklin and I. B. Wilkinson, *Eur. Heart J.*, 2014, **35**, 1719.

31 Y. S. Fang, Y. J. Zou, J. Xu, G. R. Chen, Y. H. Zhou, W. L. Deng, X. Zhao, M. Roustaei, T. K. Hsiai and J. Chen, *Adv. Mater.*, 2021, **33**(2), 20.

32 Z. D. Liu, J. K. Liu, B. Wen, Q. Y. He, Y. Li and F. Miao, *Sensors*, 2018, **18**(12), 4227.

33 P. M. Nabeel, J. Jayaraj and S. Mohanasankar, *Physiol. Meas.*, 2017, **38**, 2122–2140.

34 X. Ran, F. Luo, Z. Lin, Z. Zhu, C. Liu and B. Chen, *Nano Res.*, 2022, **15**(6), 5500–5509.

35 S. Yang, Y. P. Zhang, S. Y. Cho, R. Correia and S. P. Morgan, *Opt. Quantum Electron.*, 2021, **53**, 20.

36 G. Slapnicar, N. Mlakar and M. Lustrek, *Sensors*, 2019, **19**, 17.

37 J. Li, H. Jia, J. Zhou, X. Huang, L. Xu, S. Jia, Z. Gao, K. Yao, D. Li and B. Zhang, *Nat. Commun.*, 2023, **14**, 5009.

38 X.-R. Ding, Y.-T. Zhang, J. Liu, W.-X. Dai and H. K. Tsang, *IEEE Trans. Biomed. Eng.*, 2015, **63**, 964–972.

39 F. Miao, N. Fu, Y.-T. Zhang, X.-R. Ding, X. Hong, Q. He and Y. Li, *IEEE J. Biomed. Health Inf.*, 2017, **21**, 1730–1740.

40 F. Miao, Z.-D. Liu, J.-K. Liu, B. Wen, Q.-Y. He and Y. Li, *IEEE J. Biomed. Health Inf.*, 2019, **24**, 79–91.

41 J. Liu, B. P. Yan, Y.-T. Zhang, X.-R. Ding, P. Su and N. Zhao, *IEEE Trans. Biomed. Eng.*, 2018, **66**, 1514–1525.

42 P. Samartkit, S. Pullteap and O. Bernal, *Measurement*, 2022, **196**, 111211.

43 W.-H. Lin, F. Chen, Y. Geng, N. Ji, P. Fang and G. Li, *Biomed. Signal Proc. Control*, 2021, **63**, 102198.

44 Q. Zhang, L. Shen, P. Liu, P. Xia, J. Li, H. Feng, C. Liu, K. Xing, A. Song and M. Li, *Composites, Part B*, 2021, **226**, 109365.

45 S. Min, D. H. Kim, D. J. Joe, B. W. Kim, Y. H. Jung, J. H. Lee, B.-Y. Lee, I. Doh, J. An, Y.-N. Youn, B. Joung, C. D. Yoo, H.-S. Ahn and K. J. Lee, *Adv. Mater.*, 2023, **35**, 2301627.